Advances in Science and Technology Research Journal

Advances in Science and Technology Research Journal, 2026, 20(6), 457–472
https://doi.org/10.12913/22998624/218986
ISSN 2299-8624, License CC-BY 4.0

Received: 2026.02.06
Accepted: 2026.04.15
Published: 2026.05.01

Post-processing of guided waves using 2D-FFT for hidden defect detection in steel pipes

Drissi Azdine[1*], Elallami Mhammed[1], Tajmouati Abdelali[1]

[1] Laboratory EMIT, Department of Applied Physics, Faculty of Science and Technology, Hassan 1st University, Settat, Morocco
* Corresponding author's e-mail: a.drissi@uhp.ac.ma

ABSTRACT

This paper presents a signal processing technique for guided ultrasonic waves in a singlelayer hollow steel cylinder. The semi-analytical finite element (SAFE) method is used to compute dispersion curves for axisymmetric modes. Three-dimensional finite element modeling of L(0,1) and T(0,1) guided modes in a steel pipe with an internal defect is performed. The 2D fast Fourier transform is used for post-processing of the displacement field predicted by FE modeling in order to compute the power coefficients of the reflected and transmitted guided modes by the hidden defect. Energy conservation is demonstrated with errors below 1% across all defect depth ratios. The numerical findings are validated against established results from the published literature. Based on sensitivity, dispersion characteristics, and signal clarity, T(0,1) emerges as the most suitable mode for practical inspection of hidden defects in steel tubular structures.

Keywords: guided waves, nondestructive testing, steel pipe, SAFE method, 2D-FFT, tubular structure, mode conversion.

INTRODUCTION

Guided waves of ultrasonic waves are highly utilized in non-destructive evaluation and structural health monitoring because of their ability to travel long distances while still being sensitive to defects of relatively small sizes, as suggested by Rose [1] and Zhang [2]. This property is the basis for the use of ultrasonic waves in the inspection of hollow structures, as suggested by Quy et al. [3] and Bartoli [4]. Hollow structures may be subjected to internal and surface-related damage, which cannot be inspected using conventional inspection methods, as suggested by Fromme et al. [5].

Steel pipes are of critical importance for various applications, especially for oil and gas transportation, water supply systems, and construction engineering. Detection of defects inside steel pipes is of utmost importance for ensuring structural integrity and avoiding major failures. Changes in dispersion characteristics and redistribution of wave energy can create difficulties for defect detection, as emphasized by Rosenkrantz et al. [6]. Among axisymmetric modes of guided waves, modes L(0,1) and T(0,1) are predominantly employed for pipe inspection due to low attenuation and favorable propagation characteristics, as emphasized by Djili and Boubenider [7] and Benmeddour et al. [8]. However, interaction of these modes with internal defects inside hollow cylinders is of critical importance and demands detailed investigation. Positions of defects and input frequencies play a major role in reflection, transmission, and mode conversion phenomena, as emphasized by Soleimanpour and Ng [9] and Yan et al. [10]. Thus, mode selection is an important part of inspection methodology rather than an automatic process, as emphasized by Yan et al. [11] and Zhou et al. [12].

While numerical simulations result in a physically consistent wave response, the performance of guided wave inspection largely relies on the processing of the resulting signals. Frequency-wavenumber analysis using the

two-dimensional fast Fourier transform (2D-FFT) provides an unambiguous representation of dispersive characteristics, as demonstrated by Nissabouri [17] and El Allami et al. [18]. The 2D-FFT technique enables direct extraction of mode amplitudes and wavenumbers from spatio-temporal displacement fields.

Apart from qualitative analysis, reflection and transmission coefficients are herein regarded as quantitative indicators of mode sensitivity to hidden defects. These coefficients offer a physically meaningful means of comparing guided wave modes, as established by Cheng and Cheng [19], Long and Loveday [20], and Le et al. [21]. From an inspection point of view, this comparison is particularly important for determining which mode provides the most reliable defect detection capability.

Despite the significant progress made in guided wave inspection, a clear gap remains in the systematic comparison of axisymmetric guided wave modes for hidden defect detection in steel pipes using frequency-wavenumber analysis. Most existing studies focus on a single mode or rely on time-domain interpretation, which can be ambiguous when mode conversion occurs. Furthermore, quantitative evaluation of reflection and transmission coefficients through 2D-FFT post-processing has not been fully exploited for comparing the inspection performance of L(0,1) and T(0,1) modes in cylindrical waveguides. This motivates the present study, which aims to provide a rigorous, quantitative framework for mode selection in pipe inspection based on energy-based coefficients derived from 2D-FFT analysis. It should be noted that the present study is limited to a single pipe geometry and a single excitation frequency of 100 kHz; the applicability of the findings to other geometries and frequency ranges remains to be investigated in future work.

The main contributions of this work are threefold: (1) computation of dispersion curves for axisymmetric modes L(0,1) and T(0,1) in a single-layer steel hollow cylinder using the SAFE method; (2) quantitative analysis using 2D-FFT for mode identification and defect detection based on reflection and transmission coefficients; and (3) identification of the optimal guided wave mode for hidden defect detection in steel tubular structures.

SEMI-ANALYTICAL FINITE ELEMENT METHOD

This section presents the semi-analytical finite element (SAFE) method used to compute the dispersion curves of ultrasonic guided waves in the steel tubular structure. The theoretical framework is first described, followed by the resulting dispersion curves for the axisymmetric modes of interest.

Theoretical framework

We used the semi-analytical finite element (SAFE) approach to plot the dispersion curves of ultrasonic guided waves propagating in our single-layer steel tubular structure. A sample of the structure with all the mechanical and geometric properties is shown in Figure 1 and Table 1.

With the SAFE method, the dispersion curves for any hollow cylindrical structure can be calculated, which involves analyzing and using finite element method techniques. In this paper, a single-layer steel hollow cylinder with the geometry provided in Table 1 is used to show the dispersion curves. It adopts a cylindrical coordinate system (r, θ, z), with the z-axis aligned along the centerline of the tube. For guided waves propagating in the positive z-direction, the displacement field takes the form [1]:

$$\boldsymbol{u}(r,\theta,z,t) = \boldsymbol{U}(r,\theta)e^{i(kz-\omega t)} \tag{1}$$

where: $U(r, \theta)$ represents the cross-sectional displacement amplitude, k is the axial wavenumber, and ω is the angular frequency. In this expression, $u(r, \theta, z, t)$ denotes the displacement vector field, t is the time, and z is the axial coordinate along the pipe.

For axisymmetric modes (circumferential order $n = 0$), the circumferential dependence vanishes, and the problem reduces to a one-dimensional discretization along the radial direction. Thus, the cross-sectional domain through the wall thickness is divided into a system of radial elements, modeled using 1D finite elements with three nodes (see Figure 2).

Within each finite element, the cross-sectional displacement is approximated using shape functions $N_j(r)$:

$$U(r) = \sum_{j=1}^{n} N_j(r)U_j \tag{2}$$

Table 1. Geometric and material properties of the steel pipe

Parameter	Value	Unit
Longitudinal velocity V_L	5850	m/s
Shear velocity V_T	3200	m/s
Density ρ	7850	kg/m³
Inner radius R_{int}	50	mm
Outer radius R_{out}	60	mm
Wall thickness e	10	mm
Tube length L	2000	mm

where: U_j denotes the nodal displacement amplitudes.

Using Hamilton's principle, the equation of motion for the cross-section in its linear form can be written as [22]:

$$(A - \omega^2 M)Q = 0 \tag{3}$$

where:

$$A = K_1 + k\hat{K}_2 + k^2 K_3, Q = [\hat{U} \quad k\hat{U}]^T \tag{4}$$

where: $\omega = 2\pi f$ represents angular frequency, k denotes the wavenumber, and T is the symbol for matrix transpose.

The global stiffness and mass matrices are assembled from element contributions:

$$M = \bigcup_{e=1}^{N_{el}} m^{(e)}, K_n = \bigcup_{e=1}^{N_{el}} k_n^{(e)}, n = 1,2,3 \tag{5}$$

where: N_{el} denotes the number of elements.

The elementary matrices for cylindrical coordinates include the additional factor r from the Jacobian:

$$k_1^{(e)} = \int B_1^T C_e B_1 r dr \tag{6}$$

$$k_2^{(e)} = \int (B_1^T C_e B_2 - B_2^T C_e B_1) r dr \tag{7}$$

$$k_3^{(e)} = \int B_2^T C_e B_2 r dr \tag{8}$$

$$m^{(e)} = \int N^T \rho_e N r dr \tag{9}$$

$\hat{K}_2$ and $\hat{U}$ represent the K_2 symmetric real matrix and the cross-sectional mode shape or the new displacement vector, respectively. In Equations 6–8, the matrices B_1 and B_2 are the strain-displacement relation matrices that relate the strain components to the nodal displacements in the radial and axial directions, respectively. They are derived from the differential operators acting on the shape functions within the cylindrical coordinate framework. C_e denotes the elasticity matrix of element e, and ρ_e is the material density of element e.

For any frequency obtained by solving Equation 3, the phase velocity V_p can be deduced using:

$$V_p = \omega/k \tag{10}$$

Furthermore, Equation 3 leads to calculating the group velocity V_G as follows:

$$V_G = \frac{\partial \omega}{\partial k} = \frac{\Phi_R^T K' \Phi_R}{2\omega \Phi_R^T M \Phi_R} \tag{11}$$

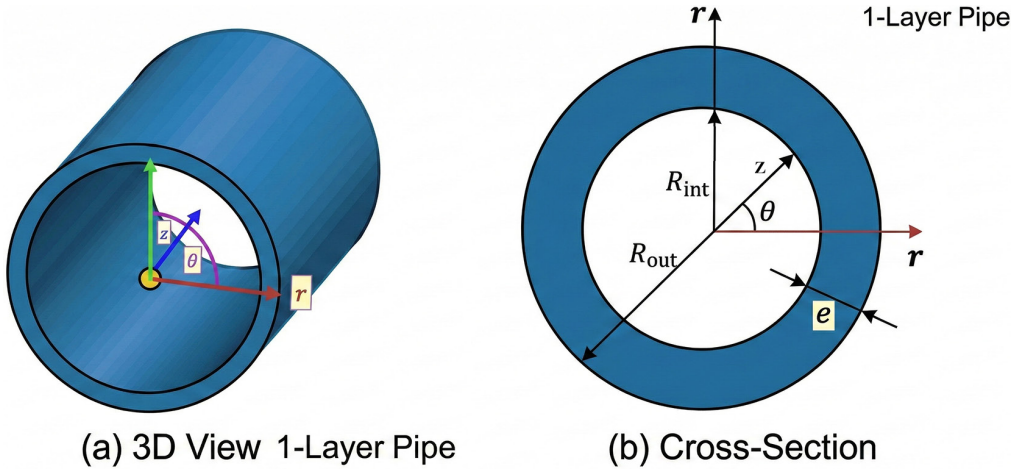

Figure 1. Schematic representation of the single-layer steel tubular structure: (a) 3D view and (b) cross-section showing inner radius R_{int}, outer radius R_{out}, and wall thickness e

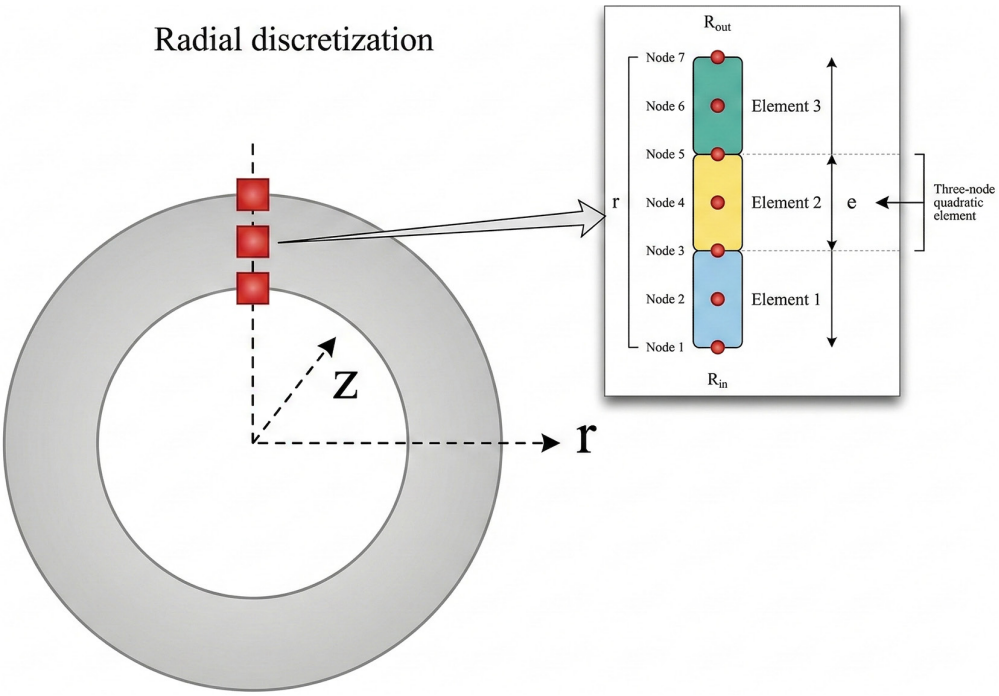

Figure 2. One-dimensional finite element discretization through the tube wall thickness showing three-node quadratic elements (with nodes represented as dots) and the cylindrical coordinate system (r, θ, z)

where: Φ_R denotes the right eigenvector of the system (i.e., the mode shape vector obtained from the eigenvalue solution of Equation 3 and K' is defined by:

$$K' = \hat{K}_2 + 2kK_3 \tag{12}$$

The dispersion behavior of ultrasonic guided waves in the steel tubular structure is explored to calculate the dispersion curves. For this purpose, this paper provides a computational framework that summarizes the major steps that constitute the process for writing a code in MATLAB to provide the numerical representation for predicting the dispersion curves and corresponding mode shapes for the steel tubular structure via the SAFE method (see Figure 3).

For hollow cylindrical waveguides, guided wave modes are classified into three families based on their displacement characteristics. Longitudinal modes $L(n, m)$ are characterized by dominant axial (u_z) and radial (u_r) displacements. For $n = 0$ (axisymmetric), these are denoted L(0,1), L(0,2), etc. Torsional modes $T(n, m)$ are characterized by purely circumferential (u_θ) displacement. The fundamental $T(0,1)$ mode is non-dispersive in homogeneous pipes. Flexural modes $F(n, m)$ are non-axisymmetric modes ($n \geq 1$) with coupled displacements in all directions.

The SAFE method efficiently computes all mode families by selecting appropriate displacement components for each circumferential order n. In this paper, we will concentrate on and plot only the axisymmetric modes of interest for pipe inspection: the fundamental longitudinal mode L(0,1) and the fundamental torsional mode T(0,1).

Dispersion curves

The entire procedure is implemented in MATLAB, providing a flexible and efficient framework for computing dispersion curves and their corresponding mode shapes. The numerical solution of Equation 3 yields dispersion curves for longitudinal and torsional guided wave modes. Figure 4 presents these curves: (a) phase velocity $C_p(f)$, (b) group velocity $C_g(f)$, and (*c*) wavenumber k.

In relation to the application of appropriate modes for effective guided wave inspection, it is essential to evaluate the characteristics of each mode for effective inspection. Both modes considered in this study have different characteristics, which make them more suitable for inspecting different types of defects. The fundamental mode of longitudinal wave L(0,1) is present at all frequencies and is considered the simplest propagating disturbance in a hollow cylinder. For

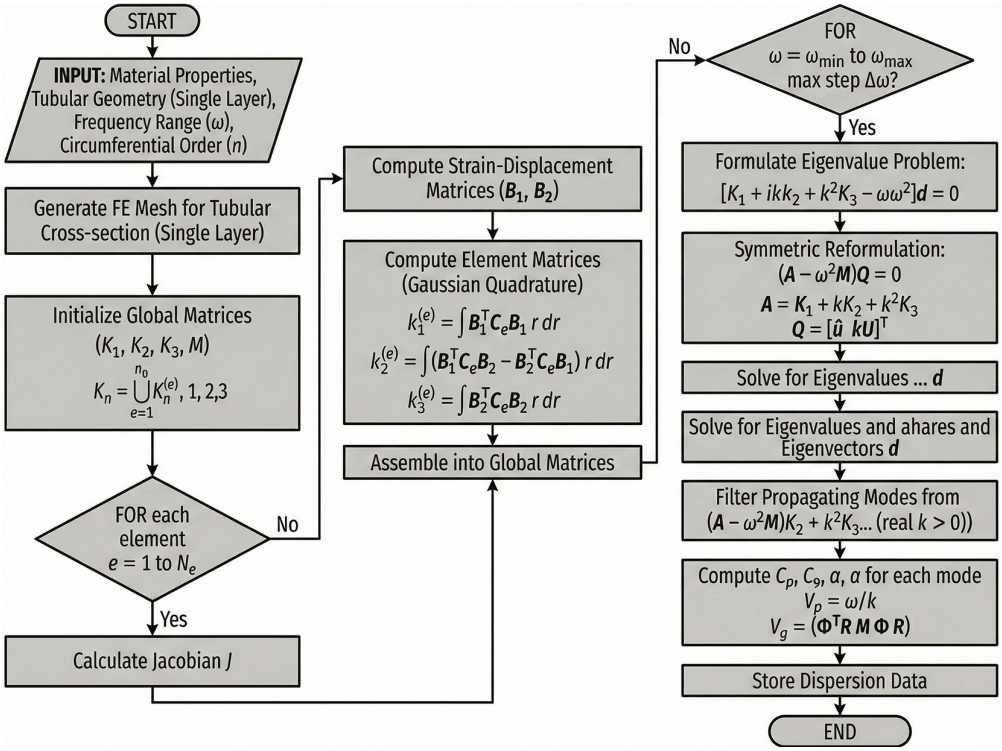

Figure 3. Semi-analytical finite element algorithm flowchart for computing dispersion curves in the steel cylinder

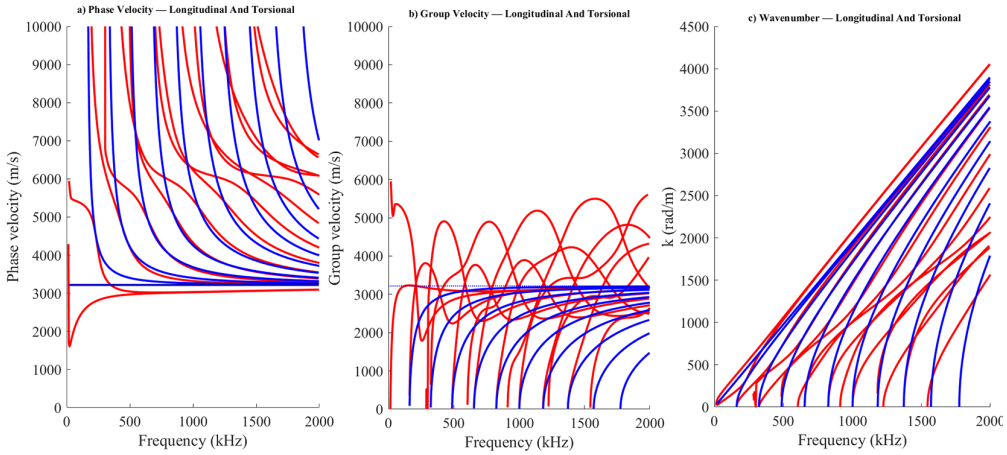

Figure 4. Dispersion curves for torsional (blue lines) and longitudinal (red lines) guided wave modes: (a) phase velocity $C_p(f)$; (b) group velocity $C_g(f)$; (c) wavenumber $k(f)$

low-frequency operation, it is observed that there is predominantly axial particle displacement with moderate dispersion. These characteristics of the fundamental mode of longitudinal wave make it more suitable for screening applications.

Because of its purely circumferential particle displacement and, for a homogeneous steel pipe, its nondispersive nature, the torsional mode T(0,1) is unique among other modes of guided waves. This feature of the T(0,1) mode is highly desirable for effective inspection, especially for long-range applications where the characteristics of the waveform are essential.

NUMERICAL STUDY

This section describes the three-dimensional finite element model constructed in ABAQUS/Explicit to simulate guided wave propagation and scattering by internal defects in the steel pipe. The model configuration, excitation strategy, and

resulting displacement fields are presented in the following subsections.

Model configuration

To investigate guided wave scattering by a hidden defect, we construct a three-dimensional finite element model of the steel pipe using commercial software (ABAQUS/Explicit). The geometric and material parameters are summarized in Table 1.

The notch depth d varies from 1.0 mm to 9.0 mm, denoting depth-to-wall-thickness ratios d/e ranging from 0.1 to 0.9, where e = 10 mm representing the wall thickness of the steel pipe. The axial extent of the notch h = 4 mm represents the axial length of the circumferential notch (see Figure 5 for a visualization of the h dimension).

The notch is circumferential around the whole tube cross section, maintaining the axisymmetric nature of the problem. The defect is located at z = 1000 mm from the excitation end, allowing sufficient propagation distance for mode development before its point of contact with the defect and adequate separation between incident, reflected, and transmitted wave packets around the monitoring locations. The mesh employs eight-node hexahedral elements with reduced integration (C3D8R). Following established guidelines for wave propagation modeling, we ensure at least 20 elements per minimum wavelength [2]:

$$\Delta x \leq \frac{V_{T,\min}}{20 f_{\max}} \approx 0.16 \text{ mm} \tag{13}$$

Equation 13 defines the theoretical upper limit of the element size based on the minimum shear wave velocity. For the proposed model, the element size of 0.83 mm was used, satisfying this requirement and resulting in the creation of nearly 38 elements within the minimum wavelength at a frequency of 100 kHz, far exceeding the recommended minimum of 20 elements within the wavelength. The explicit time integration method demands a time increment that is stable and meets the CFL requirement. For the proposed model, the element size of 0.83 mm and the maximum velocity of the wave in the steel pipe (V_L = 5850 m/s) were used to automatically calculate the stable time increment using the ABAQUS/Explicit code (approximately 0.14 μs). The total time duration was set at 1.0 ms to ensure the complete propagation of the incident pulse, the interaction between the pulse and the defect, and the separation of the reflected and transmitted pulses at the monitoring points. The finite element model consists of nearly 12 million C3D8R elements. The mesh convergence test was conducted by comparing the results from the element sizes of 1.0 mm and 0.83 mm; the difference in the results for the reflected and transmitted coefficients was less than 0.5%, confirming the suitability of the proposed mesh density for the modeling of the wave propagation at the frequency of 100 kHz.

Excitation strategy

Generating a pure guided wave mode requires applying the correct displacement profile across the inlet cross-section. We use the mode shapes computed by the SAFE method, normalized to unit power flow (Figure 6), as the spatial excitation pattern at z = 0.

The temporal waveform is a 5-cycle Hanning-windowed tone burst centered at 100 kHz [23]:

$$s(t) = \frac{1}{2}\left[1 - \cos\left(\frac{2\pi f t}{N}\right)\right] \sin(2\pi f t) \tag{14}$$

This windowed signal provides good compromise between frequency selectivity (narrow bandwidth) and temporal compactness (enabling separation of incident and scattered wave packets). The 100 kHz excitation frequency was chosen according to several factors: 1) both modes of interest L(0,1) and T(0,1)) propagate at this frequency and this is

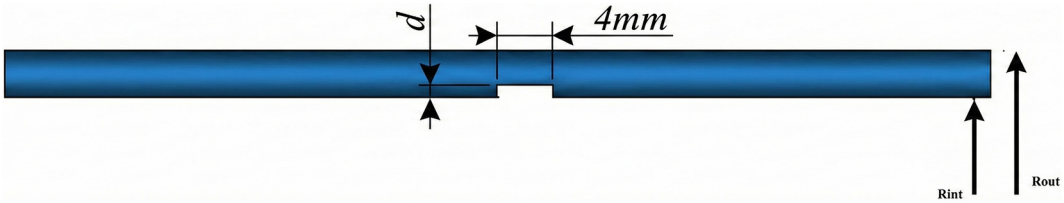

Figure 5. Schematic of the single-layer steel pipe with an internal circumferential defect, showing the axial defect extent h = 4 mm and depth d

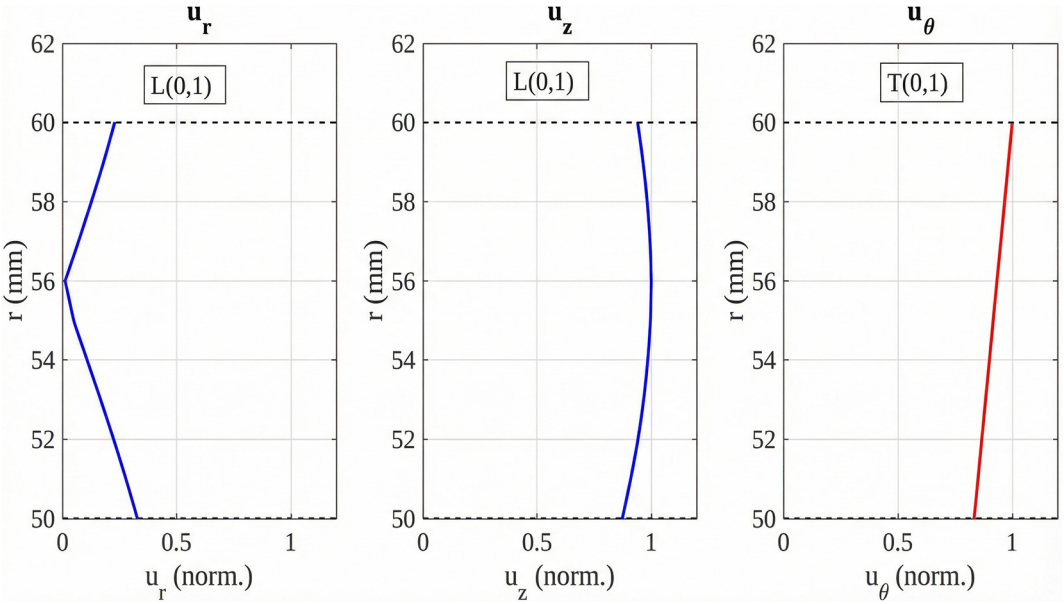

Figure 6. Normalized displacements u_r and u_z, u_θ, at f = 100kHz

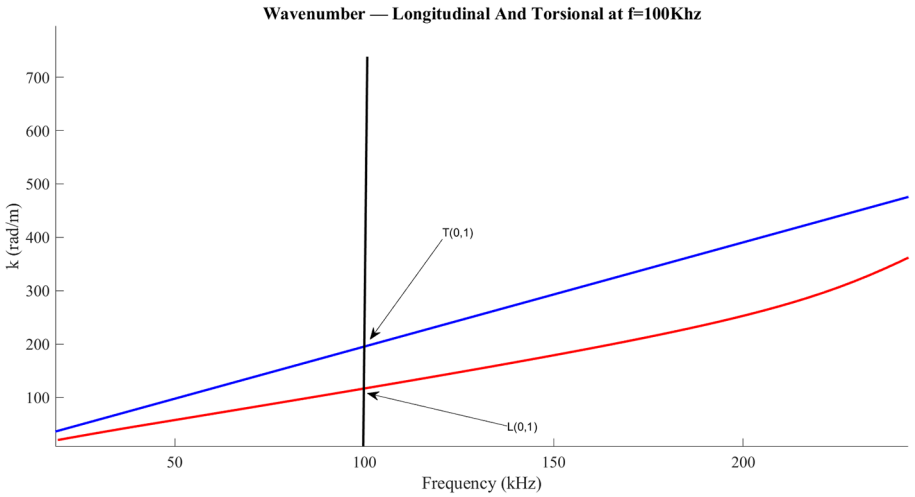

Figure 7. The adopted frequency product excitation at f = 100 kHz

confirmed through the wavenumber curve in Figure 7; 2) this frequency provides reasonable wavelengths for the finite element mesh while keeping sensitivity for the defect sizes investigated (d/e: 0.1 to 0.9); 3) at 100 kHz , dispersion of group velocity for the T(0,1) is minimal so that we can easily propagate wave packets; and 4) the 5-cycle Hanning-windowed tone burst offers sufficient frequency selectivity (bandwidth ≈ 40 kHz) without compromising temporal compactness to separate incident and scattered wave packets, aligned with established guided wave excitation in pipes. The spatial distribution of the displacements is applied as a 5-cycle tone burst weighted by a Hanning window centered on the excitation frequency (Figure 8). The selected excitation frequency is f = 100 kHz (Figure 7), chosen to ensure that both modes of interest propagate while maintaining manageable wavelengths for the finite element mesh. For this frequency, the wavenumbers of modes L(0,1) and T(0,1) are respectively $k_L(0,1)$ = 116 rad/m and $k_{T(0,1)}$ = 196 rad/m as determined from the SAFE-computed wavenumber curve presented in Figure 7. This selective single-mode excitation approach ensures that only the intended mode propagates into the waveguide, avoiding complications from multi-mode excitation that would otherwise require signal decomposition before defect interaction analysis

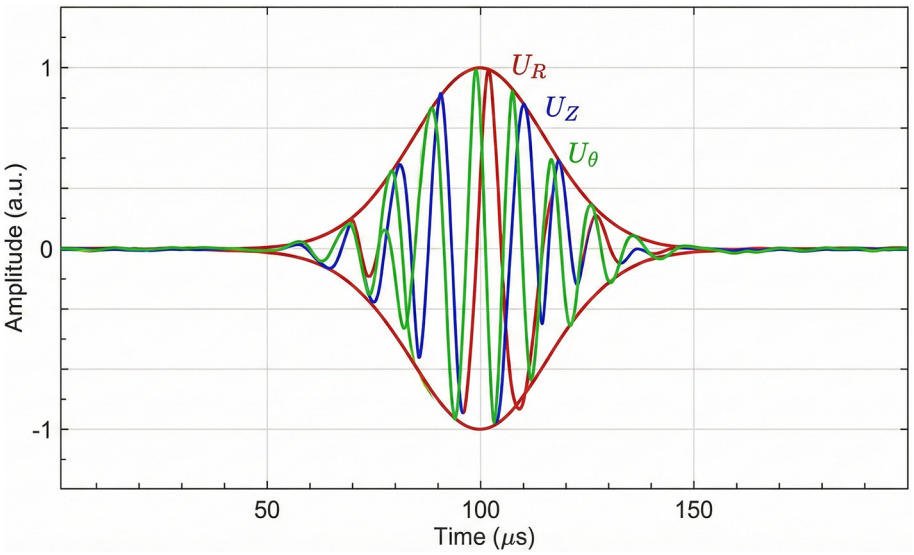

Figure 8. The temporal waveform is a 5-cycle Hanning-windowed tone burst centered at 100 kHz

Displacement fields of guided modes

Two sets of monitoring nodes were recorded on the outer surface of the steel pipe. These monitoring nodes are evenly spaced and have a spacing of 0.5 mm. These monitoring nodes were placed far enough from the ends of the tube and from the defect location to prevent non-propagating and evanescent modes, ensuring that only propagating modes are monitored. Nodes placed before the defect (at approximately 440 mm from the defect location) monitor incident and reflected modes, whereas those placed after the defect (at approximately 1120 mm from the defect location) monitor transmitted modes. The displacement signals before and after the defect, for the excitation of guided modes T(0,1) and L(0,1), are represented on the position-time plane for 100 kHz and d/e = 0.4. In these representations, it is possible to easily identify the wave packets of incident, reflected, and transmitted modes. In the case of mode T(0,1), as shown in Figures 9a and 9b, it is possible to identify the parallel ridges of the incident and reflected wave packets, indicating that there is consistency in phase and group velocity and, consequently, no mode conversion. Additionally, it is possible to identify

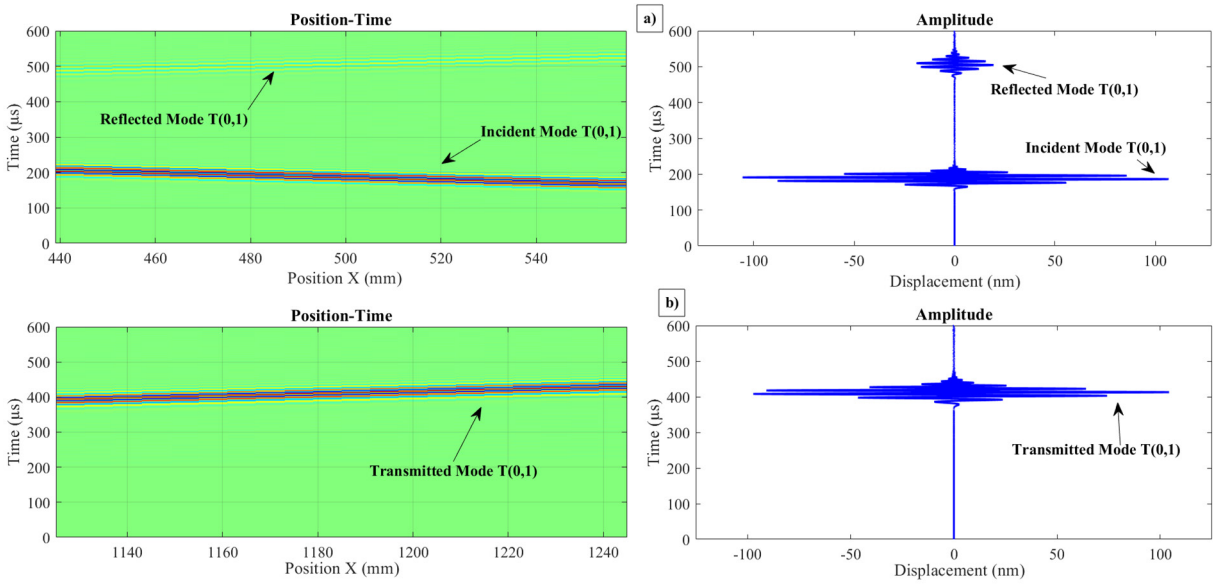

Figure 9. Displacement field for T(0,1) mode: (a) incident and reflected waves, (b) transmitted waves

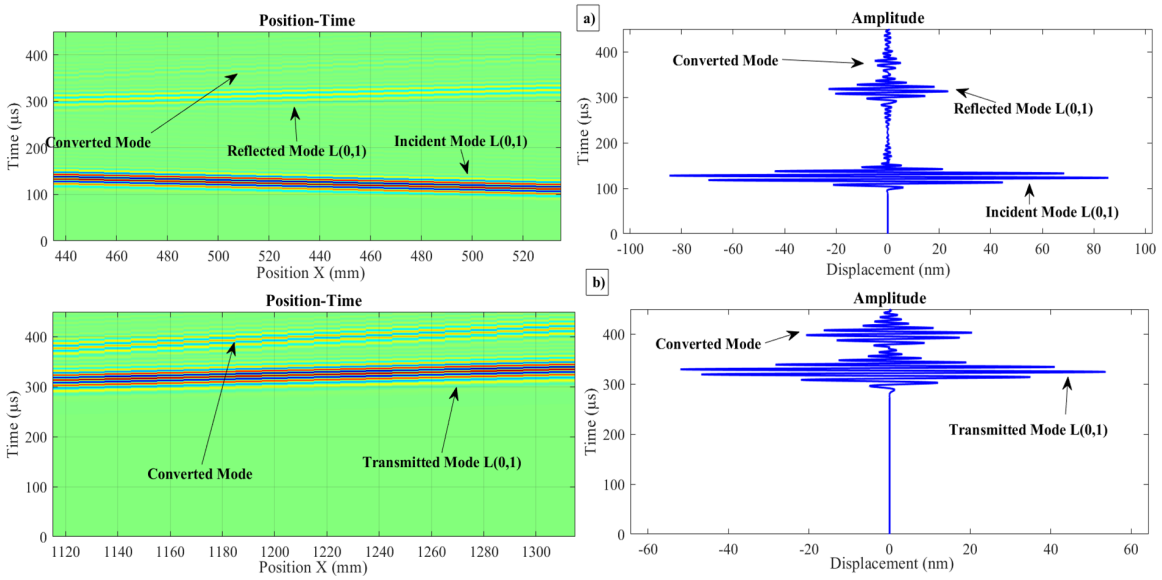

Figure 10. Displacement field for L(0,1) mode: (a) incident and reflected waves, b) transmitted waves

the same slope of the reflected and incident wave packets, indicating that there is preservation of modal characteristics for the torsional mode after interaction with the axisymmetric defect. Similarly, it is possible to identify the transmitted T(0,1) mode with a similar parallel ridge pattern, indicating single-mode propagation. For the L(0,1) mode, as shown in Figure 10, the wave packets show predominantly parallel ridges, indicating that the fundamental longitudinal mode largely maintains its modal identity. However, closer examination reveals additional features suggesting the presence of mode conversion, which will be confirmed through two-dimensional fast Fourier transform analysis in the following section.

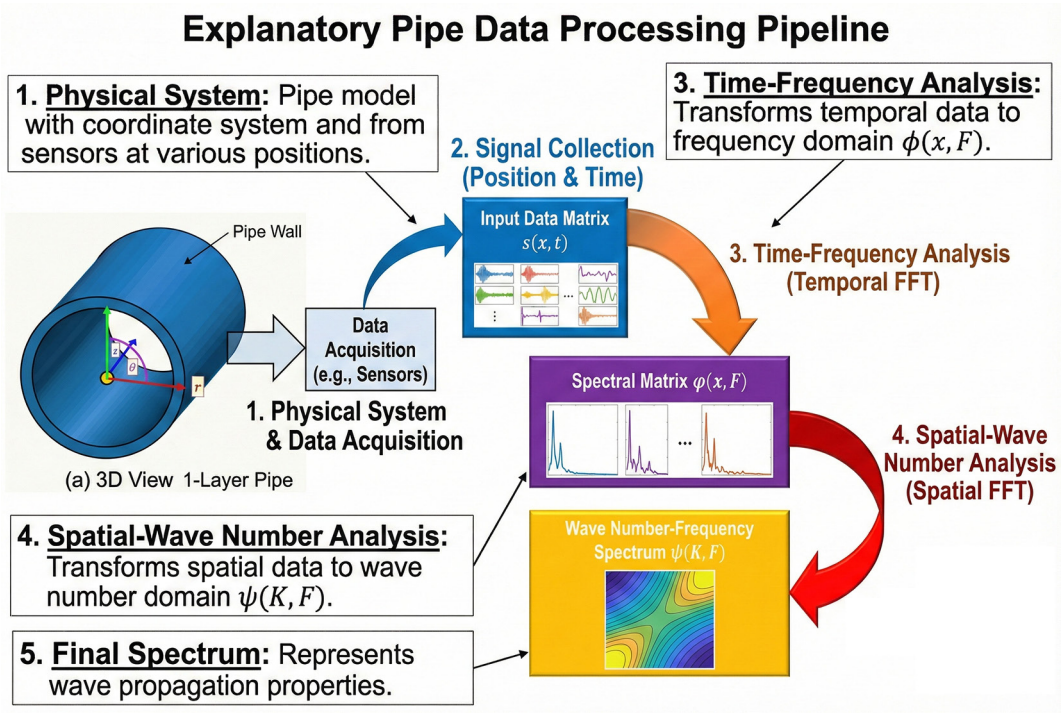

Figure 11. Processing steps for 2D-FFT analysis

POST-PROCESSING: 2D-FFT ANALYSIS

This section presents the two-dimensional fast Fourier transform (2D-FFT) technique applied to post-process the displacement signals obtained from the finite element simulations. The methodology is first introduced, followed by the results and discussion including mode identification and computation of power reflection and transmission coefficients.

Methodology

The 2D-FFT technique transforms the spatio-temporal displacement field $u(z,t)$ recorded along the cylinder surface into the frequency-wavenumber domain $\tilde{U}(k,f)$, enabling direct extraction of dispersion curves. The transformation is defined as [18]:

$$\tilde{U}(k,f) = \int_{-\infty}^{\infty}\int_{-\infty}^{\infty} u(z,t)e^{-i2\pi ft}e^{-ikz}dzdt \quad (15)$$

To identify the existing modes in the structure after reflection and transmission, we applied the two-dimensional fast Fourier transform (2D-FFT) to the displacements recorded before and after the defect to obtain the spectrum in the wavenumber-frequency (k, f) space. Figure 11 shows the processing steps to obtain the result. Figures 12 and 13 show contour plot representations of the obtained spectra. An artificial superimposition of the SAFE-computed dispersion curves onto these spectra is performed to identify the incident modes ($k > 0$), reflected modes ($k < 0$), and transmitted modes ($k > 0$).

RESULTS

Figures 12a–d illustrate the contour plot spectrum of the displacements at the monitoring zone when the incident mode is T(0,1). The 2D spectrum for the incident-reflected region (Figure 12b) shows energy concentrated exclusively on the T(0,1) dispersion branch for both positive wavenumbers (incident mode) and negative wavenumbers (reflected mode). Similarly, the transmitted spectrum (Figure 12d) shows energy only on the T(0,1) branch. These figures clearly demonstrate that no mode conversion occurs; the reflected and transmitted modes consist solely of the incident T(0,1) mode. A cut of the (k, f) representation performed at f = 100 kHz is shown in Figures 12a and 12c, displaying the amplitudes of incident and reflected T(0,1) with distinct peaks at their respective wavenumbers.

However, the L(0,1) mode exhibits fundamentally different scattering behavior. Figures 13a–d present the contour plot spectrum with L(0,1) as the incident mode. The 2D spectrum for the incident-reflected area (Figure 13b) shows that in addition to the incident L(0,1) mode,

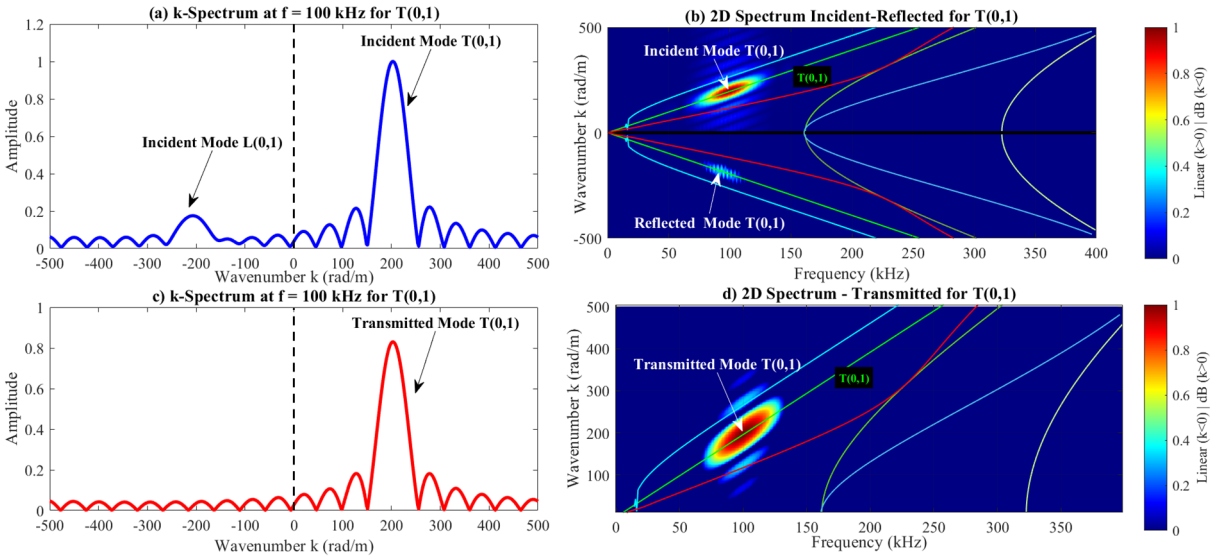

Figure 12. Analytical dispersion curves overlaid on 2D-FFT energy distribution for displacement signals before and after of the defect for incident T(0,1) mode at f = 100 kHz (d/e = 0.4): (a) amplitude normalized (incident-reflected), (b) 2D spectrum (incident-reflected), (c) amplitude normalized (transmitted), (d) 2D spectrum (transmitted)

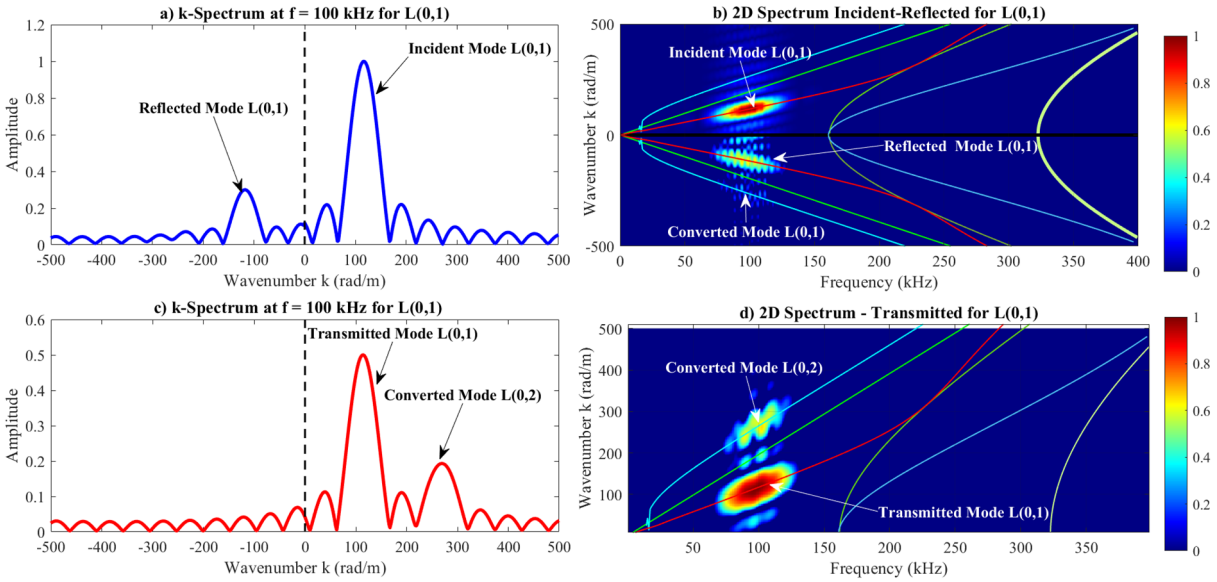

Figure 13. Analytical dispersion curves overlaid on 2D-FFT energy distribution for displacement signals before and after of the defect for incident L(0,1) mode at f = 100 kHz (d/e = 0.4): (a) amplitude normalized (incident-reflected), (b) 2D spectrum (incident-reflected), (c) amplitude normalized (transmitted), (d) 2D spectrum (transmitted)

energy is present on the L(0,2) dispersion branch at negative wavenumbers, implying partial mode conversion during reflection.

The k-spectrum at 100 kHz (Figure 13a) also supports this assertion, showing three clear peaks corresponding to the incident L(0,1), reflected L(0,1), and converted L(0,2) modes. The transmitted field corresponding to the L(0,1) mode (Figure 13d, transmitted spectrum) shows stronger mode conversion, where energy is distributed between the transmitted L(0,1) and the converted L(0,2) modes. The k-spectrum (Figure 13c) shows the main peak corresponding to the transmitted L(0,1) mode and the peak corresponding to the converted L(0,2) mode at the wavenumber of the converted mode. This mode conversion shows that the structure supports multiple modes when the L(0,1) mode is excited, namely the incident L(0,1) mode, reflected L(0,1) mode, reflected converted L(0,2) mode, transmitted L(0,1) mode, and transmitted converted L(0,2) mode. These two-dimensional fast Fourier transform representations enable unambiguous identification of the propagating modes in the steel pipe containing an internal defect when each axisymmetric mode is excited at f = 100 kHz. The spectral amplitudes extracted from the wavenumber spectrum slices at the excitation frequency provide the foundation for quantifying energy distribution among reflected and transmitted mode contributions, thus enabling computation of power reflection and transmission coefficients.

Power coefficient calculation

The reflection and transmission energy coefficients are computed from the 2D-FFT amplitudes using the following expressions. When an incident guided wave mode interacts with a defect, guided modes are generated in the steel pipe, both upstream and downstream of the defect. The reflected R_m and transmitted T_m power coefficients of a guided wave mode m(T(0,1) or L(0,1)) are defined by [18]:

$$R_m = \frac{\Phi_m^R}{\Phi^I}, T_m = \frac{\Phi_m^T}{\Phi^I} \tag{16}$$

where the power terms are defined as:

$$\Phi^I = \left|A^I u_y^I\right|^2, \Phi_m^R = \left|A_m^R u_y^m\right|^2, \Phi_m^T = \left|A_m^T u_y^m\right|^2 \tag{17}$$

Φ^I, Φ_m^R and Φ_m^T denote the powers of the incident, reflected, and transmitted guided wave mode m, respectively. u_y^I and u_y^m represent the normalized displacements of the incident mode and mode m, and A^I, A_m^R and A_m^T correspond to the amplitudes of the incident, reflected, and transmitted guided wave mode m. These amplitudes are determined by processing the displacement signals of guided waves in the studied structure.

Figure 14 present the variation of power reflection coefficient (R), transmission coefficient

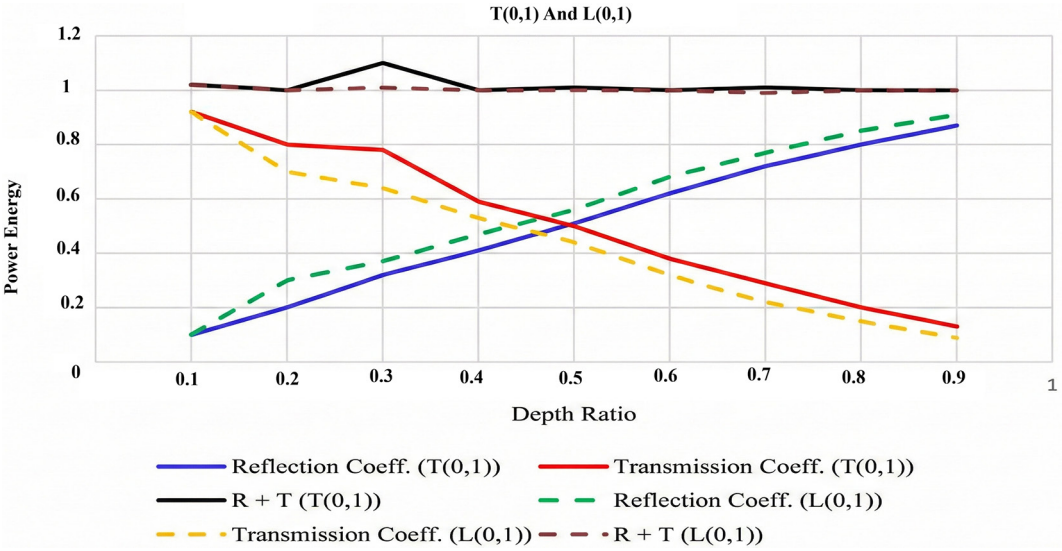

Figure 14. Power reflection and transmission coefficients for T(0,1) and L(0,1) modes as functions of defect depth ratio d/e. Energy conservation (R + T) is shown to validate the approach

(T), and their sum ($R + T$) as a function of the normalized defect depth ratio (d/e) for both axisymmetric guided wave modes: L(0,1) and T(0,1).

Both modes show perfect energy conservation, where the sum of reflected and transmitted energy is consistently close to unity for all depth ratios. For mode L(0,1), it is observed that the total amplitude of the reflection and transmission coefficients (summing contributions from both the L(0,1) and converted L(0,2) modes) is accurate to within 1% of unity, showing very accurate measurements. For mode T(0,1), it is observed that energy conservation is satisfied with negligible error, thus validating the computational approach and methodology for applying the two-dimensional fast Fourier transform post-processing. This validation is essential because it confirms that the finite element mesh is sufficiently detailed for accurate wave propagation modeling, that the monitoring locations are optimally placed for minimizing unwanted evanescent and non-propagating modes, and finally, it confirms that the two-dimensional fast Fourier transform post-processing is accurate and free of significant numerical artifacts.

Table 2. Comparative performance of guided wave modes

Criterion	L(0,1)	T(0,1)
Energy conservation	Excellent	Excellent
Defect sensitivity	Good	Good
Dispersion	Moderate	Non-dispersive
Signal Interpretation	Moderate	Simple
Long-range capability	Good	Excellent

Both modes display good sensitivity to the depth of the defects. In the case of the L(0,1) mode, the reflection coefficient varies monotonically with increasing depth from 0.08 to 0.90 as d/e varies from 0.1 to 0.9, while the transmission coefficient varies inversely. It should be noted that the monotonic relationship between the reflection coefficient and the depth of the defects makes it possible to use the L(0,1) mode to size defects, provided mode conversion effects are taken into account.

The T(0,1) mode displays analogous trends in terms of sensitivity to the depth of the defects, with the reflection coefficients increasing from 0.05 to 0.88 as d/e varies from 0.1 to 0.9. Although the reflection coefficients are slightly smaller at smaller depths ($d/e < 0.3$) compared to the L(0,1) mode, the major advantage of the T(0,1) mode is that mode conversion effects are absent, making it easier to interpret the signals. In terms of the practical use of the modes in inspection, defects with $d/e > 0.2$ have reflection coefficients > 0.15 in both modes, which should be detectable with the correct level of signal processing and noise reduction. Shallow defects ($d/e < 0.2$) are more problematic due to the smaller reflection coefficients and require higher signal-to-noise ratios to detect the defects reliably.

A comparison between the two axisymmetric guided wave modes (Table 2) shows that both modes exhibit excellent energy conservation and

good defect sensitivity. However, T(0,1) demonstrates superior characteristics for practical inspection applications due to its non-dispersive nature and simple signal interpretation.

For practical pipeline inspection, the torsional mode T(0,1) is suggested as the ideal choice for several reasons. Non-dispersive propagation means T(0,1) maintains wave packet form over long distances for accurate time-of-flight measurements and reliable defect localization. Simple signal interpretation follows since there is no dispersion effect, the analysis of reflected signals for defect characterization is significantly simpler. Adequate sensitivity shows T(0,1) has good sensitivity across all defect depths to achieve reliable detection. Long-range capability is achieved as the non-dispersive nature makes T(0,1) particularly suitable for long-range pipeline inspection applications. The L(0,1) mode shows good energy conservation and sensitivity to defects, but L(0,1) converts partially to L(0,2) during defect interaction, T(0,1) retains its modal purity and hence, its signals are clean and easy to interpret. It should be noted that these conclusions are based on numerical simulations and are validated against the published literature in the following section. Experimental confirmation of these findings is planned and would further strengthen the practical relevance of the proposed methodology.

DISCUSSION

To validate the findings of the present study, a comparison with key results from the published literature is summarized in Table 3. The comparison focuses on the main aspects investigated: reflection behavior, mode conversion, energy conservation, and mode recommendation for pipe inspection.

As can be observed from Table 3, the major findings of this research were validated by existing literature. For instance, the monotonous increase of the reflection coefficient with increasing defect depth for T(0,1) and L(0,1) modes is consistent with the 3D finite element results of Heinlein et al. [24] and Yeung and Ng [25]. Heinlein et al. [24] investigated T(0,1) reflection from defects in pipe bends and confirmed the monotonic dependence of the reflection coefficient on defect depth. Yeung and Ng [25] used a time-domain spectral finite element method to analyze torsional guided wave scattering and mode conversion from cracks in pipes, reporting similar monotonic trends. Although the pipe

Table 3. Comparison of present study findings with published literature

Aspect	Present study	Literature reference	Literature finding
T(0,1) reflection vs. depth	Monotonic increase: R = 0.05 (d/e = 0.1) to R = 0.88 (d/e = 0.9) at 100 kHz	Heinlein et al. [24]	Monotonic increase of R with depth for T(0,1) from defects in pipe bends confirmed by 3D FEM simulations
T(0,1) mode conversion at axisymmetric defect	No mode conversion observed (2D-FFT confirms energy only on T(0,1) branch)	Heinlein et al. [24]	No mode conversion at axisymmetric defects; only T(0,1) mode present in reflections
L(0,1) reflection vs. depth	Monotonic increase: R = 0.08 (d/e = 0.1) to R = 0.90 (d/e = 0.9) at 100 kHz	Yeung and Ng [25]	R increases monotonically with crack depth; spectral FEM analysis of torsional guided wave scattering in pipes
L(0,1)-to-L(0,2) mode conversion	Partial conversion observed in both reflected and transmitted fields (2D-FFT)	Yeung and Ng [25]; Huan et al. [26]	Mode conversion significant for guided waves at cracks; analytical models confirm mode-converted components at circumferential notches
Energy conservation (R + T)	R + T ≈ 1 with deviation < 1% for all d/e ratios	Ghavamian et al. [28]	FEM-based guided wave studies consistently report energy conservation as a validation criterion
T(0,1) non-dispersive advantage	T(0,1) recommended for pipe inspection: non-dispersive, no mode conversion, clean signals	Da et al. [27]; Ghavamian et al. [28]	T(0,1) preferred for defect reconstruction; widely recognized as ideal inspection mode due to non-dispersive nature and immunity to liquid loading
R governed by d/e ratio for axisymmetric defects	R depends primarily on d/e for both L(0,1) and T(0,1)	Huan et al. [26]	Analytical reflection coefficient maps as function of notch depth; d/e is the primary parameter for axisymmetric notches
SAFE + FEM approach for mode analysis	SAFE for dispersion curves + 3D FEM (ABAQUS) for scattering + 2D-FFT for post-processing	Liu et al. [29]	SAFE method for dispersion curves combined with FEM simulation for T(0,1) and L(0,2); positioning error < 1%

geometries and configurations differ from the present setup (60.3 mm outer diameter, straight pipe at 100 kHz), the fundamental reflection coefficient trends show excellent agreement.

The absence of mode conversion for T(0,1) at axisymmetric defects, as is evident from the 2D-FFT results presented in this work, is perhaps the most significant result from a practical perspective. This is also consistent with the findings of Heinlein et al. [24], where only the T(0,1) mode was observed in reflections from axisymmetric defects without any mode conversion. The mode conversion observed for the L(0,1) mode to the L(0,2) mode in this study is in accordance with the scattering and mode conversion phenomena reported by Yeung and Ng [25] for torsional guided waves interacting with cracks in pipes, and the analytical reflection coefficient models developed by Huan et al. [26] for circumferential notches. This suggestion of T(0,1) as the best mode of pipe inspection is strongly corroborated in the overall body of literature. Da et al. [27] used T(0,1) in defect reconstruction, noting the non-dispersive characteristic of the mode, while obtaining defect reconstruction errors less than 10% for defects up to half the pipe wall thickness. Ghavamian et al. [28] undertook an exhaustive review of pipe inspection using GW in the last two decades, agreeing with the prevailing consensus on the use of T(0,1) based on the insensitivity of the mode to liquid loading effects and transduction simplicity. This current research contributes further to the prevailing consensus on the best pipe inspection modes through the provision of quantitative data on the effectiveness of T(0,1), which is on par with the effectiveness of L(0,1).

The main novelty of this study in comparison to the above-cited literature can be described as the introduction of a unified 2D FFT post-processing technique that can be used to simultaneously perform mode identification, energy distribution, and coefficient calculation. While previous studies mainly focused on time-domain analysis of the signals or analytical/finite element method (FEM)-based calculations, the 2D FFT method proposed in this work can be used to directly and unambiguously visualize the energy distribution among propagating modes in the frequency-wavenumber domain, which has not been done in a systematic way in order to compare the performance of L(0,1) and T(0,1) in steel pipes.

CONCLUSIONS

The numerical investigation of ultrasonic guided wave propagation and internal defect detection in a single-layer steel pipe is discussed in detail in this paper. The dispersion characteristics of guided waves were calculated using the SAFE method and 3D simulation of guided wave interactions with concealed internal defects using ABAQUS/Explicit software. The results show that the 2D-FFT method is effective in analyzing guided wave signals in steel tubular structures, as energy conservation errors are less than 1%, proving its reliability in practical applications.

The interaction of different guided wave modes with concealed internal defects is also discussed in detail in this paper. The fundamental longitudinal mode L(0,1) is found to be suitable for defect detection applications, as it is robust and sensitive for all defect depths. The fundamental torsional mode T(0,1) is found to be the most suitable mode for defect detection in steel pipes, as it is non-dispersive and its signal is clear and easily understood with adequate sensitivity for all defect depths. The results obtained using the 2D-FFT method are robust and provide a clear framework for mode identification in the frequency-wavenumber domain. The incident, reflected, and transmitted waves are clearly identified and easily distinguished from each other. The power reflection and transmission coefficients are also obtained from the 2D-FFT spectrum and are useful for assessing defect severity.

It is worth mentioning here that some limitations are associated with this paper. The numerical simulation is carried out for a single pipe geometry and a single excitation frequency of 100 kHz. The results are not compared with available experimental results or numerical results obtained from different codes. The numerical simulation will be carried out for different pipe geometries and different excitation frequencies in the future. The results will be validated experimentally using piezoelectric transducers on steel pipe specimens and will be a valuable addition to this paper.

REFERENCES

1. Rose J.L. Ultrasonic Guided Waves in Solid Media. Cambridge University Press, Cambridge, UK; 2014.
2. Zhang X. Numerical simulation and experimental investigation on ultrasonic guided waves in

multilayered pipes based on SAFE. J. Mech. Eng. 2014; 50(8): 9–17.

3. Quy H.N., Nguyen T., Phien T.D., Phan H. Scattering of guided waves by interfacial delamination in aerospace composite laminates. In: Proceedings of International Conference on Advanced Mechanical Engineering, 2024: 585–592.
4. Bartoli I. Structural health monitoring by ultrasonic guided waves. Ph.D. dissertation, Department of Structural Engineering, University of California, San Diego, CA, USA; 2007.
5. Fromme P., Reymondin J., Masserey B. High frequency guided waves for disbond detection in multilayered structures. Acta Acust. United Acust. 2017; 103(6): 932–940.
6. Rosenkrantz E., Bottero A., Komatitsch D., Monteiller V. A flexible numerical approach for non-destructive ultrasonic testing based on a time-domain spectral-element method. NDT & E Int. 2019; 101: 72–86. https://doi.org/10.1016/j.ndteint.2018.09.001
7. Djili S., Boubenider F. Propagation of guided waves in a hollow circular cylinder: Application to non-destructive testing. EPJ Web Conf. 2010; 6: 15004. https://doi.org/10.1051/epjconf/20100615004
8. Benmeddour F., Laguerre L., Treyssede F. Scattering of guided waves from discontinuities in cylinders: Numerical and experimental analysis. In: AIP Conference Proceedings 2012; 1430: 1521–1528. https://doi.org/10.1063/1.4716380
9. Soleimanpour R., Ng C. Mode conversion and scattering analysis of guided waves at delaminations in laminated composite beams. Smart Struct. Syst. 2015; 2(3): 213–236.
10. Yan F., Qi K.X., Rose J.L., Weiland H. Ultrasonic guided wave mode and frequency selection for multilayer hybrid laminates. Mater. Eval. 2010; 68(2): 169–175.
11. Yan F., Qi K.X., Rose J.L., Weiland H. Delamination defect detection using ultrasonic guided waves in advanced hybrid structural elements. In: AIP Conference Proceedings 2010; 1211: 1563–1570.
12. https://doi.org/10.1063/1.3362254
13. Zhou S., Yao P., Xu C., Hu X. Multi-mode testing for delamination defects of composite materials using ultrasonic guided waves. In: Proceedings of IEEE Far East NDT New Technology and Application Forum (FENDT), Qingdao, China; 2019: 6–10. https://doi.org/10.1109/FENDT47723.2019.8962702
14. Capriotti M., Galvis L.W.E., Spada A. Improved global–local method for ultrasonic guided wave scattering predictions in composite waveguides and defects. J. Nondestruct. Eval. Diagn. Progn. Eng. Syst. 2023; 6(3): 031005. https://doi.org/10.1115/1.4056890
15. Srivastava A., di Scalea F.L. Quantitative structural health monitoring by ultrasonic guided waves. J. Eng. Mech. 2010; 136(8): 937–944. https://doi.org/10.1061/(ASCE)EM.1943-7889.0000136
16. Baronian V., Lhemery A., Jezzine K. Hybrid SAFE/FE simulation of inspections of elastic waveguides containing several local discontinuities or defects. In: AIP Conference Proceedings 2011; 1335: 183–190. https://doi.org/10.1063/1.3591855
17. Capriotti M., di Scalea F.L., Spada A. The global–local approach for damage detection in composite structures and rails. In: Lecture Notes in Civil Engineering 2020; 127: 831–839. Springer, Cham, Switzerland. https://doi.org/10.1007/978-3-030-64594-6_80
18. Nissabouri S. Conversion of ultrasonic waves with symmetric notches in isotropic plate. In: Proceedings of IEEE International Conference on Innovation Research in Applied Science, Engineering and Technology (IRASET), Marrakech, Morocco; 2023: 1–6.
19. El Allami M., Rhimini H., Sidki M. Application of the complex mother wavelet Shan 1–1.5 processing to Lamb modes signals in plates. Int. J. Sci. Res. 2015; 4(1): 1849–1854.
20. Cheng A., Cheng A.P. Characterization of layered cylindrical structures using axially symmetric waves. J. Nondestruct. Eval. 1999; 18(4): 117–126. https://doi.org/10.1023/A:1022632622627.
21. Long C.S., Loveday P.W. Analysis of guided wave scattering due to defects in rails using a hybrid FE–SAFE method. In: AIP Conference Proceedings 2013; 1511: 238–245. https://doi.org/10.1063/1.4789074
22. Le D., Nguyen B.K., Le T.H., Pham Q.C. Reciprocity-based closed-form solutions to guided waves in multilayered structures subjected to time-harmonic excitations. Eur. J. Mech. A/Solids 2023; 102: 105083. https://doi.org/10.1016/j.euromechsol.2023.105083
23. Azkour M., El Allami M., Rhimini H. Calculation of the dispersion curves modeling the propagation of ultrasonic Lamb waves in a bonded aluminum/epoxy/aluminum structure using the semi-analytical finite element method. Eng. Trans. 2024; 72(1): 85–102.
24. Joseph R., Yu L., Giurgiutiu V. Excitation and propagation of guided waves in multilayer hollow cylinders using PWAS transducers: A theoretical and experimental study. J. Acoust. 2020; 2: e200003. https://doi.org/10.20900/joa20200003
25. Heinlein S., Cawley P., Vogt T.K. Reflection of torsional T(0,1) guided waves from defects in pipe bends. NDT&E Int. 2018; 93: 57–63. https://doi.org/10.1016/j.ndteint.2017.09.007
26. Yeung C., Ng C.T. Time-domain spectral finite element method for analysis of torsional guided waves

scattering and mode conversion by cracks in pipes. Mech. Syst. Signal Process. 2019; 128: 305–317. https://doi.org/10.1016/j.ymssp.2019.04.013

27. Huan H., Liu L., Liu J., Huang L., Wang H., Mandelis A., Peng C. Modeling of axisymmetric ultrasonic waves reflected from circumferential notches in a pipe based on a rigorous analytical theory and implementation on distributed devices. J. Nondestruct. Eval. 2024; 43(3): 79.https://doi.org/10.1007/s10921-024-01095-0
28. Da Y., Dong G., Wang B., Liu D., Qian Z. An analytical approach to reconstruction of axisymmetric defects in pipelines using T(0,1) guided waves. Appl. Math. Mech. (Engl. Ed.) 2020; 41(10): 1479–1492. https://doi.org/10.1007/s10483-020-2661-9
29. Ghavamian A., Mustapha F., Baharudin B.T.H.T., Yidris N. Detection, localisation and assessment of defects in pipes using guided wave techniques: a review. Sensors 2018; 18(12): 4470. https://doi.org/10.3390/s18124470
30. Liu Z., He C., Wu B., Wang X., Yang S. Location detection and numerical simulation of guided wave defects in steel pipes. Appl. Sci. 2024; 14(22): 10403. https://doi.org/10.3390/app142210403